PNNL-15058

Pacific Northwest
National Laboratory
Operated by Battelle for the
U.S. Department of Energy

# The Influence of Selected Liquid and Soil Properties on the Propagation of Spills Over Flat Permeable Surfaces

J. M. Keller
C. S. Simmons

February 2005

Prepared for the U.S. Department of Energy
under Contract DE-AC05-76RL01830

PACIFIC NORTHWEST NATIONAL LABORATORY
*operated by*
BATTELLE
*for the*
UNITED STATES DEPARTMENT OF ENERGY
*under Contract DE-ACO6-76RLO183O*

PNNL-15058

# The Influence of Selected Liquid and Soil Properties on the Propagation of Spills over Flat Permeable Surfaces

J. M. Keller
C. S. Simmons

February 2005

Prepared for the U.S. Department of Energy
under Contract DE-AC05-76RL01830

Pacific Northwest National Laboratory
Richland, Washington 99352

# Summary

## Spill Spreading Area Indicates the Liquid Volume

This report develops a model for estimating the amount of liquid involved in a soil surface spill from its observed spreading area. Provided the spreading area is detectable by remote spectroscopic methods then the spill volume can be estimated. This study shows that the soil type must also be known to make such a connection.

## Selection of Example Liquids and Soils

Example organic liquids and soils were chosen to study typical spill behavior. The emphasis is on liquids that are relatively non-evaporating under normal temperature conditions. A rationale for selecting each liquid is discussed in the report.

This report also describes liquid and soil properties identified in the physical model that control spill phenomenology on permeable soil surfaces. These properties are the liquid's density, viscosity, surface tension, and wettability or contact angle; and for soils, they are the porosity, permeability, and the water-retention capability. The essential liquid and soil properties were tabulated for 10 liquids and 4 soils. The liquids constituted an array of organic chemicals, all of which are to be documented in the liquid spectra library taken at Pacific Northwest National Laboratory. The soils were chosen based on ongoing surface spectra work and to represent a range of typical soil properties. Soil properties listed in this report emphasize mainly the hydraulic behavior governing absorption of the liquids.

Ten organic liquids, mainly with low volatility, except for toluene, where selected for consideration: bis(2-ethylhexl) phosphate, dodecane, tributyl phosphate, ethylene glycol, dimethyl methylphosphonate, thiodiglycol, n-butyl alcohol, dibutylphosphate, and Inland-19 pump oil. Vapor pressures of the 10 liquids, except for toluene at 22.5 torr, compared with 17.5 torr for water, were generally much less than 1 torr. However, the n-butyl alcohol has a vapor pressure of 5 torr. Even though toluene does not fit the test requirement of low volatility, its properties and behavior are well documented and provide a good standard liquid.

These liquids ranged in density from 0.75 to 1.18 g/mL and the viscosity ranged from 0.5 to 65 cp. Toluene has the lowest viscosity of 0.5 cp compared with 1 cp for water. Thiodiglycol has the greatest viscosity, 65 cp, even compared with the Inland pump oil with 58 cp. Surface tensions were typically between 25 and 37 dynes/cm for organics other than ethylene glycol and thiodiglycol. These latter two liquids have surface tensions above 48 dynes/cm, approaching 73 dynes/cm for water. As a result of higher surface tension, the glycols have capillary retention in soil approaching that of water.

The four selected representative soils were a clay montmorillonite, warden silt loam, quincy sand, and a coarse sand named Accusand. These ranged in permeability from $2.3\times10^{-12}$ sq. cm to $2.6\times10^{-6}$ sq. cm, from clay to coarse sand. Permeability governs how quickly liquids flow through soil under the driving force of a liquid pressure gradient. During a spill, the pool height and capillary suction determine the pressure gradient responsible for liquid absorption by infiltration and imbibition. Capillary suction is determined by liquid adhesion to soil grain surfaces, causing liquid imbibition into each soil. Capillary suction or capillary pressure in a soil is related to a liquid's surface tension and its contact angle

(wettability) with the pore-scale granular surfaces. Capillary pressure or suction is also determined by the interstices size or pore radii size. Clays have the smallest interstices and the greatest capillary suction, whereas sands with largest interstices have the opposite attributes.

## Liquid Absorption by Soils

Infiltration of liquid into a soil is attributed to the weight of the liquid, which is proportional to spill height, and it represents the consequence of the downward force of gravity. Imbibition, however, represents the influence of capillary suction or liquid absorption by adhesive forces. Imbibition can occur horizontally without the influence of gravity. Liquid entering a soil from above is generally referred to as just infiltration, involving the influence of both gravity and capillary suction.

Water-retention properties for these soils are expressed in an analytical form that permitted simulating imbibition of the 10 liquids into any of the 4 soils. A fluid-soil scaling rule was used to convert water-retention behavior into corresponding behavior for the 10 organic liquids. This rule may be inaccurate for the montmorillonite because some of the organics may change its physical structure when imbibed. This possibility requires further laboratory testing.

The disappearance of liquid spilled on any of these soils is determined by infiltration into their void volume fraction called porosity. When a liquid pools on any of these porous soils, it is drawn in by capillary imbibition and infiltration caused by the pressure head of the standing liquid's depth. Each liquid infiltrates any soil as a wetting front that advances into the pore space replacing air in an initially dry soil. The strength of the capillary imbibition is described by an effective suction head at the wetting front. Estimates of this suction head were obtained by simulating water infiltration into each soil medium by using an advanced simulator of unsaturated water flow incorporating the analytical expressions for the soil-water retention properties.

## Spill Model Design

The model used to study spill phenomenology couples overland flow described by a gravity current with the Green-Ampt infiltration model. Liquid spilled on a flat surface, but possibly tilted, is described by smooth gravity current spreading. From the simulations, liquid viscosity is found to be the main controlling property determining the amount of time a spill remains on the surface, with the vanishing time decreasing as viscosity is decreased. This is attributed to a decrease in viscosity resulting in both increased hydraulic conductivity of the soil and more rapid spreading of a spill over a soil surface. Soil permeability also controlled vanishing time with that time increasing as permeability decreased, corresponding to finer textured soils. The maximum spill area was found to be largely controlled by liquid viscosity on coarse, highly permeable soils. On less permeable soils, the maximum spill area was controlled more by the equilibrium spill height because less infiltration allows the spill to reach its equilibrium height.

Simulations with and without including capillarity (suction head at the wetting front) in the Green-Ampt infiltration model demonstrated the importance of capillarity in describing the infiltration rate in fine textured soils. In coarse textured soils, capillarity was found to be negligible in describing spill behavior due to both the soil's limited capillarity and high permeability. In this study, soils are treated as water dry, and future work will consider the influence of a soil's water content on impeding the infiltration of organic liquids. Thus, the influence of capillarity as studied here is for dry soils, specifically.

## Testing the Spill Model Using Example Liquids and Soils

To establish the nature of spills on soil surfaces, model simulations were performed with the set of selected liquids and soils having representative properties. The simulations gave a spill's spatial distribution (area and infiltration depth) with time. The height of liquid standing over the area at any moment was simulated with the spill model. On soils, liquid spreading ceases when the spilled volume completely infiltrates below the surface. However, spreading may also cease when the removal of liquid over an area by infiltration just balances the spill rate. Spreading can also be physically limited when the surface is not absolutely flat. Then the depth of the surface texture compared with the prevailing spilled liquid height can limit spreading. An absolutely flat surface, however, is imposed for evaluating spills in this hypothetical study. Also, when a spill height reaches a level equal to the height of liquid standing in equilibrium on an absolutely impermeable surface, then spreading is presumed to cease because it can not go beyond the maximum area allowed by interfacial tension and contact angle with a solid soil (having pores conceptually removed).

A spill of 55 gal. of liquid dumped in 1 minute was simulated for each liquid on each soil as an example. For toluene on Accusand, the spill would infiltrate in about 1 min, whereas thiodiglycol would enter in about 3 min. On league clay, on the other hand, being least permeable, the liquids would vanish from the surface in 16 and 1250 min, respectively. Time to vanish from the surface increases for each liquid as viscosity becomes greater for infiltration into the same soil. For these soils, vanishing time increases for any viscosity as the permeability decreases from sand to clay. Toluene gives a spill area of about 3 sq. m on Accusand, whereas thiodyglycol yields 16 sq. m. On league clay, toluene spreads to 75 sq. m, whereas thiodiglycol reaches only 69 sq. m. On clay, the thiodiglycol's spread is limited more by having less interfacial wettability.

The simulations of the 55-gal. spill show that the maximum spreading area depends little on viscosity for each soil. The maximum spreading area, therefore, is nearly independent of which liquid is spilled. For any liquid, the maximum spreading area increases as the permeability decreases. For Accusand to clay, in order of decreasing permeability, the spreading areas are 12, 45, 60, and 71 sq. m for most liquids with viscosity greater than 10 cp. The spreading area is more dependent on viscosity for values below 2 cp, say for toluene or n-butyl alcohol.

## An Actual Spill Example Evaluated

Applying the model to a tanker road spill provided an example prediction when available information about the liquid amount and soil properties is limited. Although the liquid was known to be jet fuel, the exact amount was not reported until some time after the first newspaper article provided an estimated amount. Moreover, some of the original spill's spreading area may have been covered up by sand, which was apparently placed to limit more extensive dispersal of the spill, as based on photographs of the site. This example does not constitute a controlled model verification by an experiment, but is given to demonstrate how a spill would typically be analyzed to determine relationships between the rate of spill and size of the spill area produced. For the example, the specific infiltration depth reflects directly the amount spilled when distributed over the presumed visible area. The example demonstrates the importance of knowing the actual area, as should ultimately be determined using spectroscopic survey methods. In any case, the example shows how a visible spill area can be used to estimate how much liquid may have been spilled during a certain time. For the first reported spill of 2000 gal, the spreading area on the soil off the roadway was about 1700 sq. ft. covered in about 120 sec. This was consistent with

the visible spill area seen in a site photograph. The actual spill of 3000 gal may or may not give a similar area, depending on the actual spillage rate, which was unknown. Also, some of the actual area wetted by jet fuel was apparently covered by sand, so the area was not exactly known. Given the variation of the soil surface and unknown soil hydraulic properties, here presumed sand like, the measured area and amount spilled are reasonably consistent with this simplified spill model prediction.

## Future Spill Studies

Soil and liquid properties presented by this report provide a basis for future experimental work in which spill events are initiated under controlled settings, and when spill progression is monitored. Results from future experimental work will be used to validate our current conceptual model and improve the spill model as presented in this report.

# Acronyms

| | |
|---|---|
| ADI | alternating-direction implicit (method) |
| DIPPR | Design Institute for Physical Properties |
| EMSL | Environmental and Molecular Sciences Laboratory |
| LISSP | Liquid Infrared Spectroscopy and Spill Phenomenology |
| PNNL | Pacific Northwest National Laboratory |
| STOMP | Subsurface Transport Over Multiple Phases |
| USDA | U.S. Department of Agriculture |

# Acknowledgments

The authors would like to acknowledge project manager, Jeffrey L. Hylden, for supporting this work and for his technical reviews. The authors would also like to thank Wayne C. Cosby for his editorial support.

# Contents

# Figures



# Tables

# 1.0 Introduction

The spill phenomenology task of the Liquid Infrared Spectroscopy and Spill Phenomenology (LISSP) project is focused on spills as surface behavior. This report, the third in a series, is aimed at understanding spill behavior on permeable soil surfaces where liquid infiltration into the subsurface is significant in limiting a spill's extent. Understanding spill behavior allows a unique opportunity to use a spill's spatial distribution to ascertain unknown information about a spill, such as spilled substance, spill quantity, spill rate, and when the spill occurred.

The most readily obtained spatial information is a spill's surface areal extent and, to a lesser degree, the volume of the spilled material near the surface. Ideally, one would also want to know the subsurface distribution of a spill, but that information is often difficult to obtain because of site access limitations, the destructive nature of obtaining such information, and the cost of excavation. In addition, current remote sensing capabilities only allow for delineating the surface extent or the near surface extent (top millimeter of soil) of a spill and possibly the volume held near the surface. Because of the complications of obtaining a spill's subsurface distribution, this work focuses on describing the relationship between spill volume and visible surface area for permeable surfaces such as soils and gravels and the near surface volume as a function of time.

Depending on the size of a spill and access to its site, spill areal extent information may be obtained by simply walking the spill site or may require remote sensing capabilities. Fingas and Brown (1997) and Brilis et al. (2000) offer reviews on the application of remote sensing technology for identifying the visible extent of a surface spill. Theriault et al. (2001) studied the use of remote sensing to identify liquid contaminants on surfaces.

Previous work by Pacific Northwest National Laboratory (PNNL) (Simmons et al. 2004) focused on the relationship of spilled liquid volume and visible surface area for impermeable surfaces such as pavements. In that study, a model was developed that describes two-dimensional overland flow, and it was implemented to explore relationships of liquid properties, spill rate, and surface slope on the size and shape of the liquid pool. In addition, Simmons et al. (2004) describe the coupling of the two-dimensional overland flow model with a one-dimensional infiltration model.

This report expands on the discussion of overland flow coupled with infiltration as previously derived (Simmons et al. 2004) by identifying liquid and soil properties relevant to such a problem and their affect on spill phenomenology. In addition, the liquid and soil properties necessary for describing spill behavior are tabulated for 10 liquids and 4 soils.

# 2.0 Permeable Surface Spill Phenomena

This section identifies the liquid and soil properties necessary to predict the physical behavior of a spill and are the necessary input parameters of a spill model. Only by considering the model can the importance of each property be explained. The model is key to quantifying the connection between the area observed and amount spilled. Spectroscopic survey methods would be used to determine the final spill area and likely the identity of the liquid. This would allow the required estimate of the volume spilled.

The behavior of surface spills over dry permeable surfaces is largely dominated by the viscosity of the spilled liquid and the soil permeability. This is in contrast to the previous work about spills on pavements (Simmons et al. 2004) for which interfacial properties controlled the final spill area. Interfacial tension is equally important when describing spills on water-wet permeable surfaces due to water's retentive behavior in soils, potentially resisting infiltration of a spilled immiscible organic liquid; but this phenomenon is to be addressed in a future report. This section provides a brief description of the spill model used to describe the propagation of a liquid spill on a permeable soil surface. A more complete derivation of the spill model's mathematical formulation can be found in the appendix of Simmons et al. (2004).

## 2.1 Gravity Current Equation Coupled to Green-Amp Infiltration Model

The gravity current theory for describing two-dimensional spreading over an inclined-plane (flat) surface was discussed extensively by Lister (1992), and it was identified by Hussein et al. (2002) as a method to predict the spreading of oil spills on land. In addition to surface spreading, spills on a permeable surface will infiltrate and be imbibed into the subsurface. This requires including an infiltration component describing the steady removal of the spreading-liquid volume in the theory of gravity current spreading.

Acton et al. (2001) demonstrated the coupling of a one-dimensional viscous gravity current with infiltration into a relatively deep porous medium. They applied a relatively simple infiltration model known as the Green-Ampt infiltration equation (Green and Ampt 1911) without accounting for capillary-driven imbibition. The Green-Ampt model is a simplified way of treating the complicated highly nonlinear problem of estimating unsaturated infiltration into a soil surface. The model uses the boundary condition of the height of liquid standing over the porous surface, which makes its formulation ideal for the situation of a gravity current, which is mainly characterized by its varying height as the liquid spreads.

Using Lister's (1992) equation describing two-dimensional gravity current spreading, the spill model is extended to include infiltration by coupling the model to the Green-Ampt infiltration model. This theory describes the dynamical approach to the final liquid distribution both above and below the surface. The spreading is mainly controlled by gravity via the weight (density) and by the liquid's viscosity. If the surface is only rough and relatively impermeable so that only a minor volume fraction enters the substrate, then surface tension and adhesion as reflected by an effective contact angle will determine the final liquid height for which equilibrium would be achieved (Simmons et al. 2004). For permeable surfaces, however, the volume on the surface is limited by the complete imbibing of the spilled liquid.

The equation describing two-dimensional gravity current spreading combined with simplified infiltration is:

$$\frac{\partial}{\partial t}h = R\left\{\frac{\partial}{\partial x}\left[h^3\left(\frac{\partial}{\partial x}h\right)\right] + \frac{\partial}{\partial y}\left[h^3\left(\frac{\partial}{\partial y}h\right)\right] - \gamma\left(\frac{\partial}{\partial x}h^3\right)\right\} - K\frac{\left(h + h_f + z\right)}{z} \tag{2.1}$$

where R is the effective diffusion defined as:

$$R = \frac{\rho \cdot g}{3\mu}\cos\left(\theta_{surface}\right) \tag{2.2}$$

$\gamma$ is related to the gravitation force driving a spill down slope, defined as:

$$\gamma = \tan\left(\theta_{surface}\right) \tag{2.3}$$

K is the saturated hydraulic conductivity of the subsurface defined as:

$$K = \frac{k \cdot \rho \cdot g}{\mu} \tag{2.4}$$

The terms in Equation 2.1 through 2.4 are defined as follows (with units):

$\rho$ = density (g/cm$^3$)
$\mu$ = viscosity (poise)
g = gravitational acceleration (cm/sec$^2$)
k = soil permeability (cm$^2$)
$\theta_{surface}$ = angle of surface tilt (radians)
h = spill height or head above surface, normal to surface (cm)
$h_f$ = suction head at the wetting front (cm)
z = depth of infiltration below surface (cm)
x, y = space coordinates on the tilted surface.

Equation 2.1 is solved subject to the following input condition

$$\iint\left(h + \phi \cdot z\right)dxdy = q \cdot t^{\alpha} \tag{2.5}$$

where $\phi$ = substrate porosity (-)
q = spill rate (cm$^3$/sec)
t = time (sec)
$\alpha$ = input rate parameter (-).

The q in Equation 2.5 is set to zero after the duration of the spill, and Equation 2.5 does not actually hold for all time as the condition suggests. It applies only up to the specific time when the input to a spill is complete. Thereafter, the integral of Equation 2.5 is constant. Equation 2.5 is simply the statement of the conservation of the spilled liquid volume.

The Green-Ampt model used in Equation 2.1 is

$$\phi\left(\frac{\partial}{\partial t} z\right) = K \frac{h + h_f + z}{z} \tag{2.6}$$

where all terms are previously defined.

Equation 2.1 is solved by dividing the x, y domain into cells with computation nodes or locations at the cell corners. A system of finite difference equations over nodes (or grid points) is obtained to be solved for each time. The solution is advanced in time by small time intervals or steps. The node equations are put in a form that is completely or inherently mass conservative, meaning that the entire spilled volume is always accurately accounted for in the numerical finite difference scheme. At each time, the non-linear volume balance equations are solved using a Newton-Raphson iteration procedure. Further, the system of difference equations is solved by using an alternating-direction implicit (ADI) method for a parabolic type of partial differential equations. During the solution, for each time step, the spill input and infiltration extraction are treated as sink terms in Equation 2.1. Liquid removed from above the surface according to Equation 2.6 appears as the distribution of z.

Importantly, the spill model describes stable or regular spreading phenomena and would not be applicable to unstable spreading. Unstable spreading in the form of unpredictable fingering protrusions may form with low-viscosity liquids, particularly on sloped surfaces. Imperfections and undulations on the surface can also produce or trigger irregular finger flow.

## 2.2 Summary

The equations and solution scheme described allow for the computation of stable spreading phenomena. With general knowledge of a liquid's physical characteristics of density ($\rho$) and viscosity ($\mu$), the substrate's porosity ($\phi$), permeability (k), wetting front suction head ($h_f$), and the surface slope ($\theta_{surface}$), the stable spill propagation for the liquid can be estimated for different spill rates (q) and spill quantities. Until the model is validated experimentally, this model is considered a theoretical mathematical tool that allows for estimating the effect of liquid and substrate properties on spill behavior and for guiding future experimental work. Proceeding sections discuss the liquid and substrate parameters and their effect on spill behavior.

# 3.0 Liquid and Soil Properties

The attributes of the physical parameters needed by the spill model of the prior section are explained in this section. These are the usual well-known properties of liquids and porous granular soils. These attributes must be appreciated to understand their impact on spill behavior. A list of selected liquids and soils is provided for future studies and model confirmation. A rationale for the list selection is given also.

A liquid spilled on a permeable surface, such as a soil, spreads over the surface while simultaneously infiltrating into the subsurface, acting to remove liquid mass from the surface. The rate and extent that the liquid spreads over a permeable surface is in part controlled by properties of the spilled liquid and by the rate that the liquid infiltrates into the subsurface, with the infiltration rate being controlled by both liquid and soil properties. Individual liquid and soil properties impart different influences on the spill propagation process. This section describes liquid and soil properties influencing spill behavior on permeable surfaces and provides a tabulation of properties for 10 liquids and 4 soils of interest.

## 3.1 Principal Liquid and Soil Properties

Five liquid and soil properties that are of particular importance in dictating spill propagation on permeable surfaces are presented. The discussion is modified from Simmons and Keller (2003) who presented a thorough review of spill-modeling parameters. The information needed to familiarize the reader with the parameters relevant to the spill model presented in Section 2.1 is given. If desired, additional information on these and other spill-model parameters can be found in the above reference.

### 3.1.1 Liquid Density

Liquid density is the mass of the liquid divided by the volume it occupies under the existing pressure and temperature conditions. The gravity current flow theory used to describe surface spreading is driven by the downward pull of gravity as a result of the liquid's density. Not considering the effects of viscosity, the denser a liquid, the faster its rate of spreading. On a permeable surface, an increased spreading rate will increase the liquid's degree of spreading because the liquid is capable of reaching a maximum spreading area more quickly before the loss of surface mass from infiltration causes spreading to cease either because of steady-area surface conditions or complete infiltration of the surface component of the spill.

Liquid density is also a component in describing hydraulic conductivity (K) or the rate at which the liquid will conduct through the soil, leading to its removal from the surface. As liquid density increases, the hydraulic conductivity and the infiltration rate increase. The result is that the influence of liquid density on the degree of spreading may be minimized by density's effect on the infiltration rate.

Because of the opposing effects that density has on spreading behavior and because of the greater influence of other properties, density is considered a secondary property when analyzing spill spreading behavior of a system when only air and the spilled liquid are present. In a system composed of air, the spilled liquid, and water, the density of the spilled liquid relative to the density of water, and the effect that relationship might have on the spilled liquid's surface behavior become important considerations. As an example, if a spilled immiscible liquid is less dense than water, the immiscible liquid will float on top of water. One can visualize the significance of this if the groundwater table is near the soil surface,

limiting the infiltration depth and creating the potential for the spilled liquid to remain pooled on the soil surface.

### 3.1.2 Viscosity

Viscosity is a measure of a fluid's resistance to flow due to the internal friction of a liquid. Viscosity determines how rapidly a liquid will flow over a surface as a result of forces acting on the liquid, such as gravitational force. The less viscous a fluid, the faster its rate of spreading over the surface will be. Along with intrinsic permeability and liquid density, viscosity also controls the liquid conductivity through soil with a less viscous fluid being more conductive. As with density, a less viscous liquid will flow faster overland, allowing it to cover a larger surface area before the liquid infiltrates into the subsurface and depletes the surface volume to a point where spreading stops. This effect is counteracted by the increased hydraulic conductivity of the less viscous liquid, resulting in a larger infiltration rate or rate of removal of the liquid from the subsurface. Viscosity is considered a primary property for describing spill spreading behavior because of the considerable influence viscosity has in the spill model and the large degree of variation of liquid viscosities for the chemicals of interest.

### 3.1.3 Intrinsic Permeability

Intrinsic permeability is an inherent property of a soil that relates to the cross sectional area of the pore space that permits flow through a porous medium. This can be conceptualized by considering an individual water-filled pore portrayed by a cylinder of radius r. From Poiseuille's law, when laminar flow conditions prevail, the volumetric flow rate (Q) through the pore can be approximated by:

$$Q = \frac{\pi \cdot r^4 \cdot \rho \cdot g \cdot \Delta p}{8\mu \cdot L} \tag{3.1}$$

where $\rho$ = fluid density
$g$ = gravitational acceleration
$\Delta p/L$ = pressure drop per unit distance
$\mu$ = fluid viscosity.

While the cross sectional area of a pore is proportional to $r^2$, from Equation 3.1, the flow through a pore is proportional to $r^4$. The result is that a single large pore with the same cross-sectional area of numerous small pores will conduct more water. This can be explained by the fact that a single large pore will promote less viscous drag along the pore wall than numerous small pores will. Because coarse-textured soils are generally composed of pores of larger radius than fine-textured soils, intrinsic permeability can be related to soil texture with coarser soils, such as sands having a larger intrinsic permeability than finer clay and silt soils. Intrinsic permeability varies by orders of magnitude, depending on the soils being considered, resulting in conditions in which large volumes of fluid are easily transmitted into the soil or conditions in which very little infiltration occurs. In situations where large infiltration occurs, spreading would be limited by removing spill mass from the surface. The opposite would be true under limited infiltration conditions, promoting large surface areal coverage of spills and long surface existence times.

Using a liquid's physical parameters of density and viscosity in conjunction with the soil's intrinsic permeability, the hydraulic conductivity (K) of the liquid through the soil can be derived using

Equation 2.4. A fluid and soil specific K is then used in the solution of the Green-Ampt infiltration model.

### 3.1.4 Interfacial Tension

Interfacial tension is the potential energy associated with the interfacial area of the contact between two substances. The interfacial tension between a liquid and its vapor is commonly called surface tension. Surface tension along with adhesive forces, described by a contact angle, are responsible for capillary effects in soils.

On impermeable surfaces, Simmons et al. (2004) showed that the surface coverage of a spill is determined by the equilibrium pool height or the height at which the downward pull of gravity on the spill is balanced by the internal tension of the liquid, causing the liquid to stop spreading.

On permeable surfaces, this pool height is best described as the steady-area pool height because a dynamic process persists in which even after the steady-area pool height is reached and surface spreading stops, the pool height will continue to decrease as the liquid infiltrates into the subsurface. On a soil surface, capillarity may allow a liquid to spread even more by lowering the effective surface contact angle. Alternatively, surface roughness may act to limit spreading. For the purpose of this study, capillarity's effect on the steady-area pool height was considered negligible, and the surface was regarded as absolutely flat. With these assumptions, the steady-area pool height (h) can be described using the equilibrium height relationship presented by Simmons et al. (2004):

$$h = \sqrt{\frac{[1-\cos(\beta)]\cdot\sigma}{\rho\cdot g}} \tag{3.2}$$

where $\beta$ = contact angle
$\sigma$ = surface tension
$\rho$ = liquid density
g = gravitational acceleration.

Even on permeable surfaces, the above relationship is important in determining the spill partition over an area because for fine-textured soils the permeability may be small enough to limit infiltration, causing the final maximum spreading area to be controlled by the steady-area spill height. Once the steady-area spill height is reached, the spill will no longer spread, but infiltration will continue until all surface liquid has infiltrated. Surface tensions vary little for our liquids of interest, but large variations in surface tension would have the potential to produce highly variable h values and maximum spreading areas.

An additional effect interfacial tension has on spreading behavior is if water is present within the soil matrix, the water may preferentially adhere to the soil grains and will not be easily displaced by an immiscible liquid. This condition would limit the infiltration of a spilled immiscible liquid, resulting in both larger spreading areas and longer surface pool times.

### 3.1.5 Soil-Water Retention Characteristics

Soil-water retention describes how strongly water is retained by soil when the soil-water content has a specific value. How strongly the water is held by the soil is termed the matric potential. The soil-water retention functional relationship is used with other constitutive flow relationships to determine the basic equation of liquid movement.

Scaling theory allows for a soil-water retention curve to be related to a retention curve for a different liquid by using the relationship:

$$\psi_{nw} = \psi_w \frac{\rho_w}{\rho_{nw}} \cdot \frac{\sigma_{nw}}{\sigma_w} \tag{3.3}$$

where $\psi$ = matric potential
$\sigma$ = surface tension
$\rho$ = liquid density
subscripts w and nw = water and nonwater, respectively.

For a clay soil, the scaling relationship described in Equation 3.3 may not apply for organic liquids because of both the chemical interactions between organics and highly reactive clay surfaces and the variable shrinking and swelling of clays in contact with organics of differing dielectric constants (Graber and Mingelgrin 1994; Chen et al. 1987).

A coarse-textured soil, which is composed of pores of larger radius than a fine-texture soil, will possess a smaller matric potential at a given moisture content than would a fine-textured soil. The result is that a coarse-textured soil will retain less liquid near the soil surface than a finer textured soil, with the liquid readily draining away from the near surface of a coarse-textured soil.

In addition, the soil-water retention curve describes the capillarity or the capability for the soil to wick a liquid. Capillarity increases infiltration rate by promoting the drawing in of surface liquid through enhancing subsurface liquid movement. A fine-textured soil will possess a greater liquid matric potential than a coarser textured soil, again because of the pore radius differential, resulting in increased capillarity for the fine-textured soil. Subsurface transport behavior and the removal of liquid from the soil surface remains largely dominated by the soil's intrinsic permeability, but capillarity will significantly enhance a soil's liquid transport behavior, particularly in fine soils and especially at earlier times when the depth of infiltration below the surface is at it smallest. In the Green-Ampt infiltration model, capillarity is captured by $h_f$. The $h_f$ will be specific to a particular soil and liquid and in actual field conditions will vary with depth because of nonuniform soil conditions.

For modeling purposes, it is beneficial to represent the water-retention characteristics curve in a continuous functional form. A commonly used parametric model for representing the relationship between matric potential and moisture content is the van Genuchten (1980) model described by:

$$\Theta = \frac{\theta - \theta_r}{\theta_s - \theta_r} = \left[1 + (-\alpha \cdot \psi)^n\right]^{-m} \tag{3.4}$$

where $\Theta$ = degree of saturation
$\theta$ = moisture content
$\theta_r$ = residual moisture content
$\theta_s$ = saturated moisture content
$\alpha$, n, and m = fitting parameters with m often defined as 1-1/n.

The $\alpha$ is considered to represent the inverse of the air entry pressure or the pressure at which drainage will begin.

In most cases, soils will possess two distinct water-retention curves, a drying curve and a wetting curve. An example of each is presented in Figure 3.1. A drying curve is obtained by taking a sample that is initially saturated and applying suction to desaturate the sample. The wetting curve is obtained by wetting an initially dry sample. The difference in curves is primarily a result of nonuniform pore shapes, different liquid-solid contact angles for an advancing and receding liquid, and the presence of entrapped air in soil that is being wetted. The result is that the water content in the drying curve is higher at a given matric potential than it is in a wetting curve. The infiltration of a spill would be considered a wetting scenario since the soil is initially unsaturated. Most soil-water retention curves available in the open literature are drying-type relationships. In lieu of measuring the wetting characteristic curve, Luckner et al. (1989) suggested approximating the wetting characteristics curve by

$$\alpha_{wetting} \cong 2\alpha_{drying} \tag{3.5}$$

Where $\alpha$ is the fitting parameter used in Equation 3.4, and wetting and drying correspond to the type of water-retention curve.

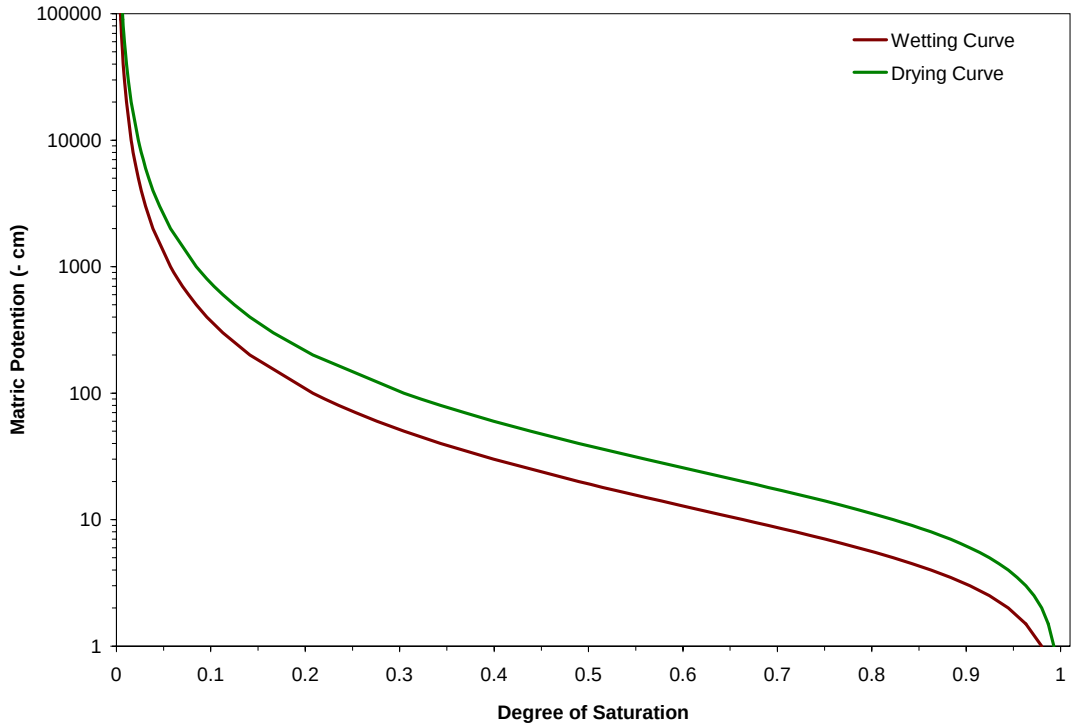


**Figure 3.1. Example Drying and Wetting Soil-Water Retention Curve**

## 3.2 Liquid Properties

Properties of liquid density, viscosity, surface tension, and vapor pressure were tabulated for the 10 liquids presented in Table 3.1. The chemicals were selected to represent a range of organics and in concert with chemicals in the liquid spectra library as measured in the Environmental Molecular Science Laboratory (EMSL) at PNNL. More specifically, bis(2-ethylhexyl) phosphate, dodecane, and tributyl phosphate were chosen to align the spill phenomenology task of the LISSP project with the surface spectroscopy work performed at EMSL. Dodecane serves as a proxy for kerosene, which is the primary component of jet fuels. Inland-19 was chosen as a surrogate for transmission fluids and motor oils based on Inland-19's CAS number being the major component of both. Toluene is included as a well characterized standard that may be used for future experimental work.

**Table 3.1. Liquids Selected for Characterization**

| Common Name | Synonyms | CAS | Chemical Formula |
|---|---|---|---|
| Bis(2-ethylhexyl) phosphate | Di(2-ethylhexyl) phosphate | 298-07-7 | $[CH_3(CH_2)_3CH(C_2H_5)CH_2O]_2PO_2H$ |
| Dodecane | Kerosene, JP-3 | 112-40-3 | $CH_3(CH_2)_{10}CH_3$ |
| Tributyl phosphate | Tri-n-butyl phosphate | 126-73-8 | $[CH_3(CH_2)_3O]_3P(O)$ |
| Ethylene glycol | Ethylene alcohol, 1,2-Diethanediol, EG, Monoethylene glycol | 107-21-1 | $HOCH_2CH_2OH$ |
| Dimethyl Methylphosphonate | DMMP | 756-79-6 | $CH_3P\text{-}O\text{-}(OCH_3)_2$ |
| Thiodiglycol | 2,2'-Thiodiethanol, B*is*(2-hydroxyethyl) sulfide | 111-48-8 | $S(CH_2CH_2OH)_2$ |
| n-Butyl alcohol | n-Butanol, 1-Butanol | 71-36-3 | $CH_3(CH_2)_3OH$ |
| Dibutylphosphate | Phosphoric acid dibutyl ester | 107-66-4 | $(CH_3CH_2CH_2CH_2O)_2P(O)OH$ |
| Inland-19 pump oil | transmission fluid | 64742-65-0 | - |
| Toluene | methylbenzene | 108-88-3 | $C_6H_5\text{-}CH_3$ |

A number of sources were used in acquiring defensible chemical properties. The two primary sources are the Design Institute for Physical Properties (DIPPR) database maintained by Brigham Young University and the Beilstein database. Where properties other than vapor pressure were not available in the open literature, they were measured by Augustine Scientific (Newbury, OH), a laboratory specializing in the measurement of surface and interface properties. Vapor pressures for two of the chemicals were unavailable and were estimated using the Solaris prediction module developed by Advanced Chemistry Development Software (Toronto, Canada).

Properties for the selected liquids are listed in Table 3.2. Water is included to allow for a basis of comparison and because its density and surface tension is needed for scaling the soil-water retention curve using Equation 3.3. Properties were taken at 20°C unless otherwise noted.

**Table 3.2. Properties of Selected Liquids**

| Common Name | Density ($g\ cm^{-3}$) | Viscosity ($g\ cm^{-1}\ s^{-1}$) | Surface Tension ($g\ s^{-2}$) | Vapor Pressure (torr) | Source |
|---|---|---|---|---|---|
| Water | 0.997 | 0.010 | 72.9 | 17.5 | DIPPR |
| Bis(2-ethylhexyl) phosphate | 0.965[a] | 0.374[a] | 28.75[a] | $1x10^{-7}$[b] | Augustine Scientific/ Estimated |
| Dodecane | 0.747 | 0.015 | 25.4 | 0.098 | DIPPR |
| Tributyl phosphate | 0.979 | 0.039 | 27.79 | 0.004 | Beilstein |
| Ethylene glycol | 1.112 | 0.207 | 48.5 | 0.058 | DIPPR |
| Dimethyl Methylphosphonate | 1.174 | 0.040[b] | 36.7 | 1.2[b] | Beilstein |
| Thiodiglycol | 1.183 | 0.652 | 54 | 0.803 | Beilstein |
| n-Butyl alcohol | 0.810 | 0.030 | 24.8 | 5.003 | DIPPR |
| Dibutylphosphate | 1.056[a] | 0.615[a] | 29.41[a] | 0.001[b] | Augustine Scientific/ Estimated |
| Inland-19 pump oil | 0.860[b] | 0.576[b] | 28[b] | $1x10^{-5}$ [b] | Manufacturer |
| Toluene | 0.870 | 0.005 | 28.5 | 22.5 | DIPPR |
| (a) Measured at 22°C<br>(b) Measured at 25°C | | | | | |

The density of the liquids ranges from a low of 0.747 g $cm^{-3}$ for dodecane to a high of 1.183 g $cm^{-3}$ for thiodiglycol. Compared to the magnitude in difference of other properties, the variation in density for the selected liquids is a minor component in the difference in spill behavior of the liquids. A potentially key difference in behavior due to density is that 6 of the 10 liquids are less dense than water, which would result in their floating on water under conditions of the soil being water saturated.

The viscosity of the liquids ranges from a low of 0.005 g $cm^{-1}$ $s^{-1}$ for toluene to a high of 0.652 g $cm^{-1}$ $s^{-1}$ for thiodiglycol. The large range in viscosities for the liquids is an important attribute, producing differences in the behavior of the spilled liquids by affecting both the surface spreading rate and infiltration rate.

Surface tensions range from 24 g $s^{-2}$ to 54 g $s^{-2}$, which are typical values for organic liquids. The differences in surface tension will not only result in small differences in the steady-area spill height on the surface, but will also change the scaling of the retention curves and $h_f$ from Equation 3.3. The result is that as surface tension increases, $h_f$ will also increase, enhancing infiltration.

Of the liquids studied, toluene possesses the largest vapor pressure, with its vapor pressure being 22.5 torr. The remainder of the chemicals have vapor pressures less than that of water, suggesting that evaporation of the liquid will be minimal at room temperatures, and, depending on the liquid infiltration behavior, surface mass loss of the liquid will primarily be caused by infiltration.

## 3.3 Soil Properties

Soil properties were collected for four soils ranging from a fine-textured montmorillonite clay soil to a uniform coarse-textured commercial sand. The clay soil and coarse sand were selected to be consistent with the two soils used in ongoing work to obtain liquid spectra for chemicals on soil surfaces. The remaining two soils, a silt loam and a fine textured sand, were selected in an effort to provide a range of soils encountered on the earth's surface.

**Table 3.3. Grain-Size Statistics and USDA Texture Classification for the Soils Studied**

| Soil | USDA Texture | Percent Sand (2-mm > 0.05-mm) | Percent Silt (0.05-mm > 0.002-mm) | Percent Clay (<0.002-mm) | Geometric Mean Particle Diameter (mm) | Geometric Standard Deviation (mm) |
|---|---|---|---|---|---|---|
| Accusand | Coarse Sand | 100.0 | 0.0 | 0.0 | 0.729 | 0.936 |
| Quincy Sand | Fine Sand | 86.9 | 10.5 | 2.5 | 0.151 | 0.425 |
| Warden Silt Loam | Silt Loam | 37.3 | 55.2 | 7.4 | 0.031 | 0.241 |
| League Montmorillonite | Clay | 9.1 | 42.4 | 48.5 | 0.001 | 0.038 |

Table 3.3 presents the U.S. Department of Agriculture (USDA) texture designation and the particle size distribution statistics for the four soils of interest. Note that because particle size is typically log-normal distributed, the particle diameter means and standard deviations are geometric (log) means and geometric (log) standard deviations.

**Table 3.4. van Genuchten Parameters and Permeability for the Soils of Interest**

| Soil | $\theta_s$ ($cm^3\ cm^{-3}$) | $\theta_r$ ($cm^3\ cm^{-3}$) | $\alpha_{drying}$ ($cm^{-1}$) | $\alpha_{wetting}$ ($cm^{-1}$) | n (-) | permeability ($cm^2$) |
|---|---|---|---|---|---|---|
| Accusand[(a)] | 0.348 | 0.016 | 0.100 | 0.200 | 10.570 | $2.6\times10^{-6}$ |
| Quincy Sand[(b)] | 0.304 | 0.036 | 0.081 | 0.162 | 1.562 | $3.8\times10^{-8}$ |
| Warden Silt Loam[(c)] | 0.496 | 0.000 | 0.020 | 0.040 | 1.325 | $8.2\times10^{-10}$ |
| League Montmorillonite[(d)] | 0.589 | 0.109 | 0.001 | 0.002 | 1.419 | $2.3\times10^{-12}$ |

(a) Schroth et al. 1996.
(b) Gee et al. 1989b.
(c) Gee et al. 1989a.
(d) Parker et al. 1985.

Table 3.4 presents the van Genuchten model parameters (Equation 3.4) and permeability for the four soils. The $\alpha_{wetting}$ was approximated using Equation 3.5. A review of Table 3.4 shows that the parameters follow the expected trends with both saturated moisture content and residual moisture content increasing as the soil texture becomes finer while $\alpha$ and permeability decrease. Permeability decreases by six orders of magnitude from the Accusand soil to the montmorillonite clay soil. As described in Section 3.1, this is due to increased viscous drag caused by the abundance of smaller radius pores in finer soils. Under a spill condition, the league montmorillonite soil would experience a minimal infiltration rate compared to that of the coarser Accusand soil. As a result, a spill on the clay soil would tend to spread further and remain on the surface for a longer period of time than an identical spill on coarser textured soil. A spill on the Accusand soil will tend to readily infiltrate into the soil, minimizing surface spreading.

Figure 3.2 shows the soil-water retention curves for each soil produced using Equation 3.4 and the parameters listed in Table 3.4. The soil-water retention curves show the coarse Accusand nearing saturation at a low matric potential and the transition from residual saturation to saturated conditions being sharp because of the nearly uniform pore sizes making up the soil. As the soils become finer, saturation conditions occur at higher matric potentials, and the transition from residual saturation to saturation is not as sharp because an increasing distribution of pore sizes are present in the soil.

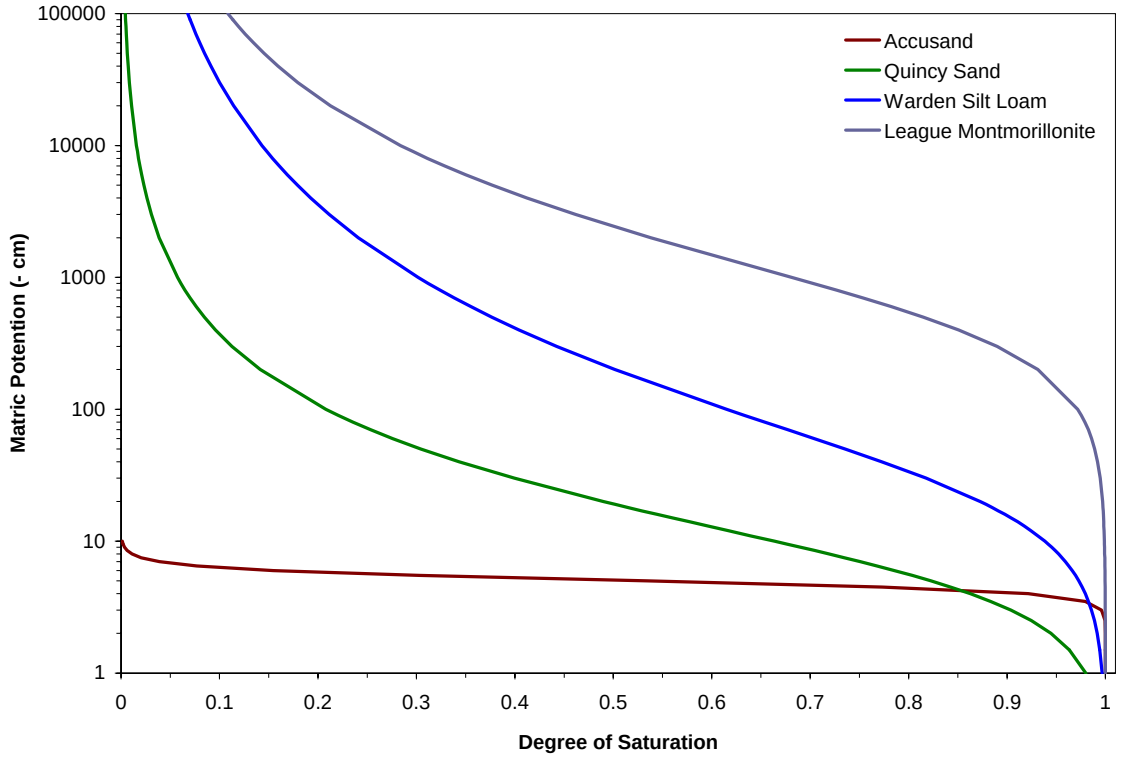


**Figure 3.2. Wetting Water Retention Curves for Soils of Interest. The large variability between curves illustrates the considerable difference in the hydraulic properties of each soil.**

A first-order estimate of soil capillarity or $h_f$ in the Green-Ampt equation can be made by identifying $h_f$ as the matric potential at which the soil reaches saturation. This matric potential is equivalent to $1/\alpha$ from the van Genuchten model. Improved approximations can be made by the mathematical methods of Neuman (1976) or by calibrating the Green-Ampt model to a more sophisticated subsurface flow model. For this report, we chose to calibrate the Green-Ampt model using the subsurface flow and transport simulator STOMP (Subsurface Transport Over Multiple Phases) (White et al. 1995). Using the van Genuchten parameters presented in Table 3.4, forward simulations of a one-dimensional infiltration event were simulated for all four soils. A saturated surface boundary condition with zero ponding was prescribed for each simulation. Using the STOMP simulated liquid-volume input, the Green-Ampt model was calibrated by adjusting $h_f$ until the Green-Ampt model calculated volume input matched that simulated by STOMP. From the calibration, $h_f$ was observed to change with time, becoming smaller as the calibration time increased. Because the effects of capillarity are most significant during early times of the spill, a calibration time of 60 seconds was chosen to best capture the effective $h_f$. The calibrated $h_f$ values for the four soils are presented in Table 3.5.

**Table 3.5. Calibrated Green-Ampt $h_f$**

| Soil | $h_f$ (cm) |
|---|---|
| Accusand | 4.4 |
| Quincy Sand | 1.4 |
| Warden Silt Loam | 10.8 |
| League Montmorillonite | 555 |

It is worth noting that the hydraulic parameters presented are highly dependent on the soil physical properties, such as packing or bulk density. The top few millimeters of a soil may have different hydraulic characteristic than the bulk soil because of exposure or modification. For example, foot and vehicle traffic often results in surface soils possessing a larger bulk density than the underlying soil matrix. In addition, eolian (wind) processes may result in a finer textured soil on the surface, or the impact of raindrops may result in surface crust formation. Such conditions would affect the infiltration behavior of the soil as a whole. For the purpose of this study, modification of the soil surface is not considered, and the soil surface is assumed to have the same hydraulic characteristics as the underlying soil. Accordingly, the hydraulic properties presented in Table 3.4 are for an ideal bulk soil sample.

## 3.4 Summary

Liquid properties of density and viscosity and soil properties of intrinsic permeability, interfacial tension, and soil-water retention are briefly described as is their anticipated effect on spill behavior. Viscosity and permeability have the greatest effect on spill propagation, in part because of their large degree of variation across different liquids and soils. Decreasing viscosity has the dual effect of both increasing spreading rate and infiltration rate, while a decreasing permeability decreases infiltration rate. A compilation of the selected liquid properties shows that for these chemicals, density and surface tension possess little variation compared to the magnitude of variation of viscosity. The vapor pressure for the tabulated liquids suggests that evaporation would be insignificant in the removal of surface liquid during a spill

event. Soil permeability for four soils varied by six orders of magnitude from the clay soil to a coarse sand soil, with the clay soil possessing the smaller permeability. This has a pronounced effect on spill behavior, with the clay soil acting much like a pavement, while the spilled liquid would readily infiltrate on a sand soil, limiting the spill area. On a highly permeable granular medium, such as course sand or gravel, the spill may hardly spread at all and merely infiltrate over the source area. In this extreme, the spill is mainly controlled by the infiltration and not by spreading.

# 4.0 Hypothetical Spill Simulations

Some implications of the liquid and soil properties listed in the previous section are given for a hypothetical spill by using the spill model to make specific predictions for a volume of one barrel spilled onto the given range of soils. The time that a liquid remains on the surface before disappearing completely captures the combined influence of these physical properties. This section helps a reader understand the consequences of the property interactions during a spill.

To determine the relative importance of both chemical and soil properties on spill propagation, spills were simulated using the spill model described in Section 2.1. A combination of liquid and soil properties from Section 3.0 were used in the simulations. Spills were simulated at a spill rate of 0.917 gal $sec^{-1}$ and a spill duration of 60 seconds, equating to a total spill volume of 55 gal. The simulations assume that before the spill, the soil system was completely dry, and the only liquid introduced to the system is that of the spilled liquid. In addition, both the surface and subsurface were assumed to be homogeneous. Using Equation 3.2, the steady-area spill heights were calculated for the chemicals, using contact angles calculated from the equation-of-state equations presented by Li and Neumann (1990). For the calculation of contact angle, a soil surface energy value of 205.1 g $s^{-2}$ (Helmy et al. 2003) was used for all soils. Table 4.1 presents the steady-area spill height for the five chemicals used in the simulations.

Table 4.2 displays the vanish time, or the time that all liquid is removed from the surface, for simulated spill events of toluene, n-butyl alcohol, ethylene glycol, bis(2-ethylhexyl) phosphate, and thiodiglycol on the four soils studied. The five chemicals cover the range of densities, viscosities, and surface tensions for the chemicals of interest. From the simulation results, vanish time is highly dependent on both the liquid viscosity and soil permeability, with vanish times increasing as viscosity increases and intrinsic permeability decreases. A plot of vanish time versus viscosity for all four soils is presented in Figure 4.1. An increase in viscosity of over two orders of magnitude from toluene, the least viscous chemical, to thiodiglycol, the most viscous chemical, results in relatively little variation in vanish times for the highly permeable Accusand.

**Table 4.1. Calculated Steady-Area Spill Heights for Simulated Spills**

| Chemical | Steady-area Spill Height (mm) |
|---|---|
| Toluene | 2.5 |
| n-Butyl Alcohol | 2.4 |
| Ethylene Glycol | 2.8 |
| Bis(2-ethylhexyl) Phosphate | 2.4 |
| Thiodiglycol | 2.9 |

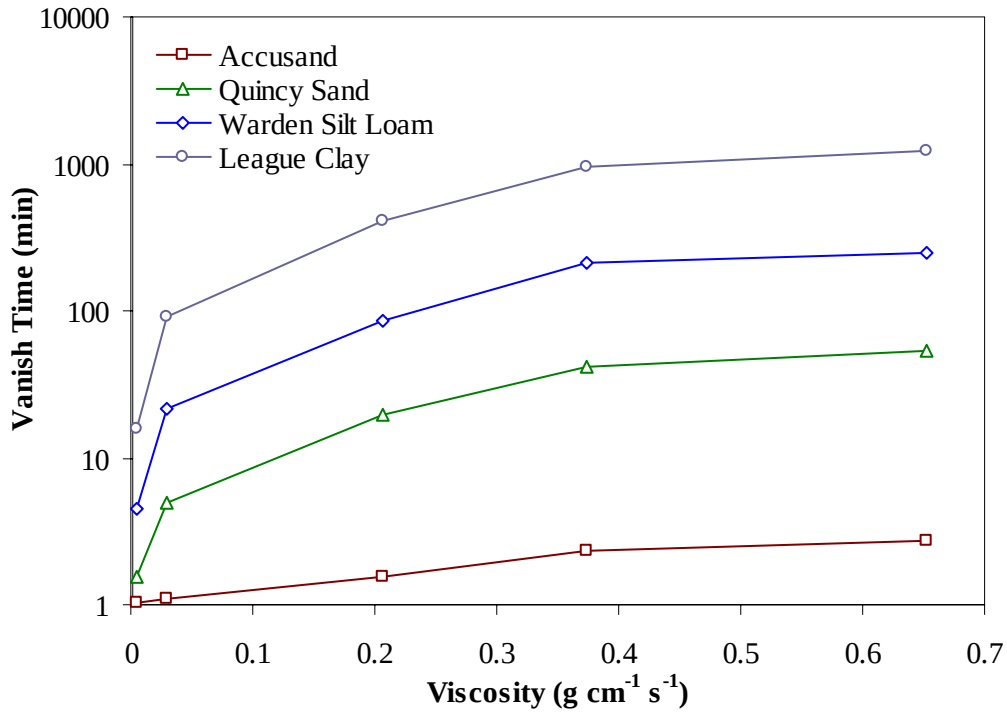


**Figure 4.1. Plot of Vanish Time as a Function of Viscosity for the Simulated Spill Events**

The opposite is observed with the clay soil in which flow is dominated by smaller radius pores. In this soil, the vanish time for thiodiglycol is nearly 80 times larger than that for toluene. The simulated trends in vanish times are expected, given that infiltration rates are largely dependent on the hydraulic conductivity of the soils, which is a product of both liquid viscosity and permeability. In addition, a lower viscosity would result in a faster surface spreading rate, increasing the surface area available for infiltration shortly after a spill has occurred. The properties of surface tension and density should affect spill behavior to some extent, but their effects are not evident because of the dominance of viscosity in spill propagation.

In addition to vanish time, the maximum surface areas covered by the simulated spill events were calculated and are presented in Table 4.3. The calculated trends in maximum spill areas is a result of the competing events of decreasing viscosity, increasing infiltration rate, and surface spreading rate, and in the case of soils with low permeability, the maximum surface area being limited by interfacial properties and the steady-area spill height. Figure 4.2 shows the maximum spill area for each soil related to the liquid viscosity. For the highly permeable Accusand, the spill has little time to spread before all the spilled liquid has entered the subsurface, making the maximum area controlled by viscosity. For the other three soils in the study, the spreading area is less dependent on viscosity for values above that of n-butyl alcohol or 0.03 g $cm^{-1}$ $s^{-1}$. Above this viscosity, the area remained nearly the same for the same soil. Thus, spills of more viscous liquids would produce similar observable areas for a particular soil and spill volume.

**Table 4.2. Vanish Time or Time of Surface Disappearance for Simulated Spill Events**

| Chemical | Density (g/cm^3) | Viscosity ($g\ cm^{-1}\ s^{-1}$) | Surface Tension ($g\ s^{-2}$) | Vanish Time (min) | | | |
|---|---|---|---|---|---|---|---|
| | | | | Accusand | Quincy Sand | Warden Silt Loam | League Clay |
| Toluene | 0.870 | 0.005 | 28.5 | 1.02 | 1.57 | 4.46 | 15.67 |
| n-Butyl Alcohol | 0.810 | 0.030 | 24.8 | 1.11 | 4.95 | 21.85 | 90.96 |
| Ethylene Glycol | 1.112 | 0.207 | 48.5 | 1.57 | 19.47 | 86.74 | 407.33 |
| Bis(2-ethylhexyl) Phosphate | 0.965 | 0.374 | 28.8 | 2.34 | 41.89 | 210.51 | 959.27 |
| Thiodiglycol | 1.183 | 0.652 | 54 | 2.71 | 53.78 | 245.11 | 1245 |

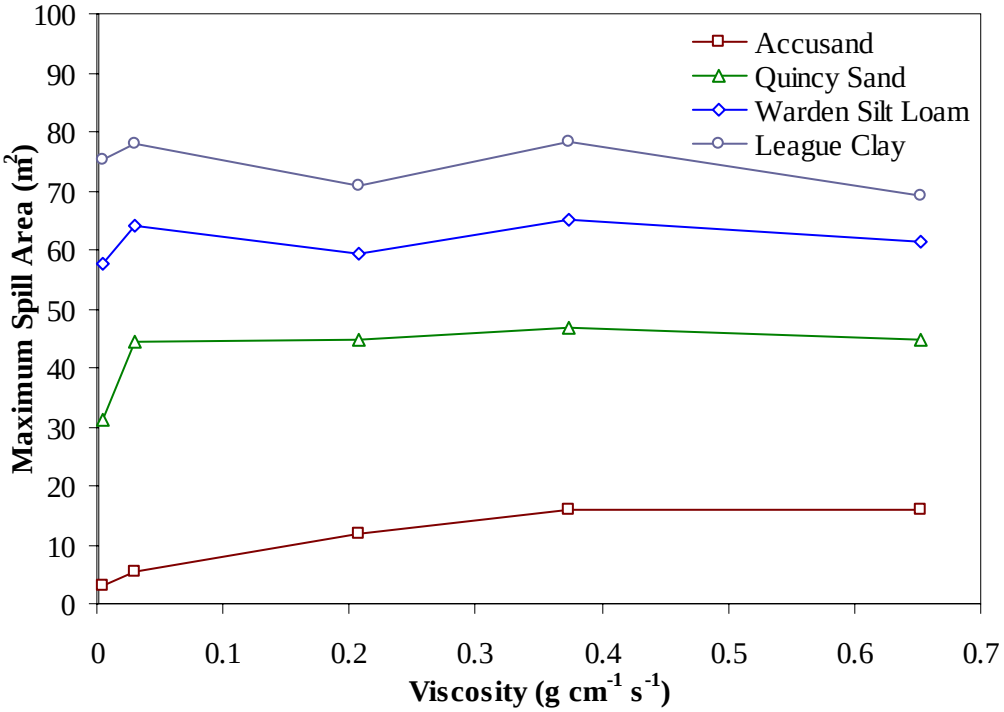


**Figure 4.2. Simulated Maximum Spill Area as a Function of Viscosity**

For low permeable soils, the steady-area spill height, or the surface pool height at which spreading stops, controls the maximum spill area. This transition occurs because the spill is no longer able to completely infiltrate before reaching the steady-area spill height. This is particularly evident looking at the maximum spreading area for the league clay soil as a function of steady-area spill height in Figure 4.3. For the league clay soil, the maximum spreading area is controlled by the steady-area spill height, with the maximum surface area decreasing with increasing steady-area spill height. Thus, the league clay will

behave much like the pavements discussed by Simmons et al. (2004) in terms of maximum spreading area.

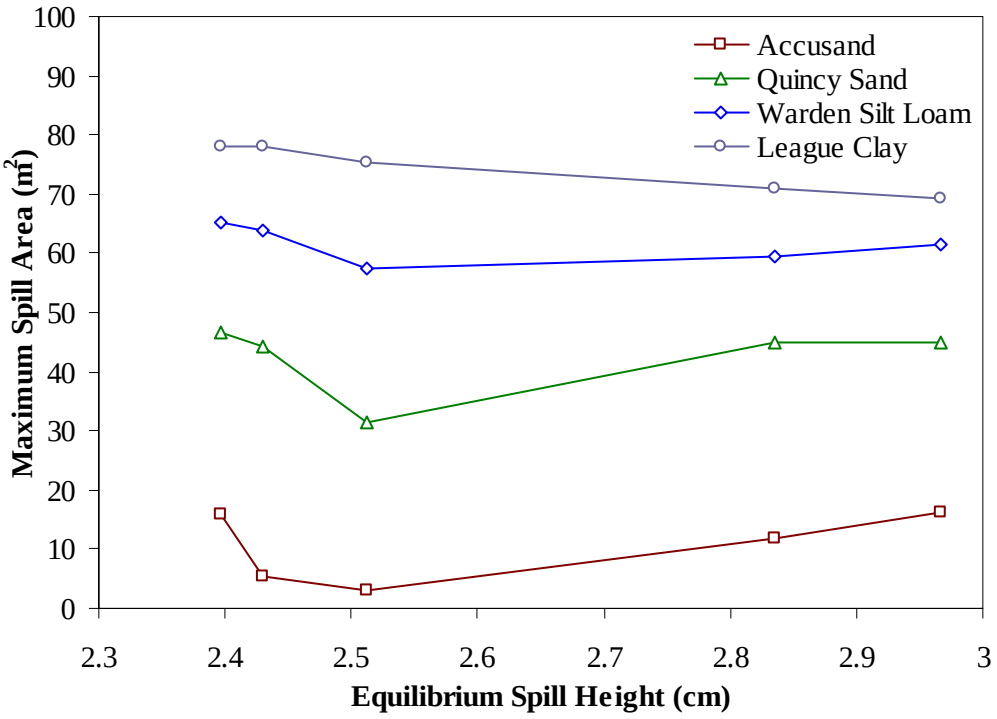


**Figure 4.3. Simulated Maximum Spill Area as a Function of Steady-area Spill Height**

The importance of capillarity in describing spill behavior was explored by performing a set of ethylene glycol spill simulations in which $h_f$ was set to equal zero, equivalent to removing the effects of capillarity. Table 4.4 presents the simulated vanish times with and without accounting for capillarity in the simulations. For the highly permeable soils, the difference in vanish times under both scenarios with and without capillarity are similar. Calculated $h_f$ for the Accusand and quincy sand were relatively low, being 4.4 cm and 1.4 cm, respectively, so this is expected. For the finer, less-permeable soils that possessed a much larger capillarity, 10.8 cm for the warden silt loam and 555 cm for the league clay, capillarity proved to be very important in describing the infiltration behavior of the spilled liquid with the vanish time on the clay soil increasing from 407 minutes to 233,600 minutes or approximately 162 days. The maximum spreading area behaved similarly as the vanish time with maximum spreading area becoming larger when not accounting for capillarity and the increase becoming more pronounced as the soil became finer. This illustrates the importance of including capillarity when simulating spill events, particularly on soils with low permeability.

**Table 4.3. Maximum Spill Area for the Simulated Spill Events**

| Chemical | Density (g/cm^3) | Viscosity ($g\ cm^{-1}\ s^{-1}$) | Surface Tension ($g\ s^{-2}$) | Maximum Spill Area ($m^2$) | | | |
|---|---|---|---|---|---|---|---|
| | | | | Accusand | Quincy Sand | Warden Silt Loam | League Clay |
| Toluene | 0.870 | 0.005 | 28.5 | 2.91 | 31.28 | 57.47 | 75.29 |
| n-Butyl Alcohol | 0.810 | 0.030 | 24.8 | 5.34 | 44.33 | 63.93 | 78.11 |
| Ethylene Glycol | 1.112 | 0.207 | 48.5 | 11.95 | 44.85 | 59.36 | 70.92 |
| Bis(2-ethylhexyl) Phosphate | 0.965 | 0.374 | 28.8 | 15.89 | 46.75 | 65.17 | 78.17 |
| Thiodiglycol | 1.183 | 0.652 | 54 | 16.10 | 44.90 | 61.32 | 69.23 |

**Table 4.4. Vanish Times for Simulated Ethylene Glycol Spill Events with and Without Accounting for Capillarity**

| Chemical | Vanish Time (min) | | | |
|---|---|---|---|---|
| | Accusand | Quincy Sand | Warden Silt Loam | League Clay |
| Ethylene Glycol With Capillarity | 1.57 | 19.47 | 86.74 | 407.33 |
| Ethylene Glycol Without Capillarity | 1.81 | 26.27 | 711.22 | 233,600 |

## 4.1 Summary

Spill simulations performed using a combination of liquid and soil properties from Section 3.0 illustrate that liquid vanish time is largely controlled by the viscosity of the liquid and the permeability of the soil. On a highly permeable soil, variations in viscosity did not produce a large effect on vanish time, but the opposite was observed on less permeable soils with vanish time showing a large increase with an increase in viscosity. Spill results indicate that an area is mainly determined by soil type, remaining nearly the same across all ranges of viscosity for the same soil. This is true mainly for liquids with viscosity much greater than that of water. Thus, the observed area for a particular volume would be about the same associated with any liquid for a particular soil. Knowing the soil, therefore, makes it possible to estimate volume from area regardless of liquid involved, at least for more viscous liquids.

The trends in simulated maximum spill area are a result of competing effects of viscosity, permeability, and interfacial properties. For highly permeable soils, the maximum spill area increased with viscosity. As permeability decreased, a transition was achieved in which the steady-area spill height, as determined by the interfacial properties, determined the maximum spreading area. This is a direct result of the infiltration rate being limited because of low permeability, allowing the spill to spread over the surface until reaching its steady-area spill height. The importance of capillarity ($h_f$) in describing spill behavior was demonstrated, most notably for fine soils possessing large $h_f$. This suggests that $h_f$ can not be neglected when modeling spills on permeable surfaces.

# 5.0 History Matching an Observed Spill Event

An actual spill case discussed here suggests how well the spill area and volume might be associated. There were many unknowns in this case for which a spill scenario had to be formed to make the estimation possible. This example is not a model verification, but only a demonstration of relationships. For instance, one finds that the measurable area in a site photograph corresponds approximately to a certain portion of the spilled quantity.

## 5.1 A Roadway Fuel Spill

A tank truck spill of jet fuel (JP-8) onto a roadway in Idaho State occurred in the summer of 2004, and the story of its potential environmental damage was reported by the Idaho Statesman (Boise, ID). It was first reported that 2000 gal of fuel was released, but later the amount was revised to be 3000 gal. Because a picture of the spill area was taken and reported in the news, this was an excellent opportunity to test the spill concepts presented in this report. The first reported amount of 2000 gal was employed along with the best estimate of visible spreading in the area to make an estimate. Unfortunately, the spreading area was likely reduced by remediation attempts using a cover of dumped sand. Thus, this example can not attempt to match an exact area with an exact spill volume.

Figure 5.1 shows a published picture of the spill site. The picture was use to estimate the surface area affected by the liquid. Using the first reported information, the modeling objective was to see if observations would be reasonably consistent with estimation of spreading.

**Figure 5.1. Picture of Jet Fuel Spill Site**

An apparent sand pile is noticeable on the upper right edge of the roadway. Some of the spill may have been covered, hiding it from the estimate based on surface darkness. Moreover, a larger scale photograph suggested that the fuel may have run downhill along the roadway for considerably more distance before being sand covered. Therefore, the exact spill area is uncertain.

From the picture, it was determined that the tank likely tipped onto the side of the road, and then the fuel ran slightly down slope toward the side where the tank trailer is shown standing. So the supposition was that the fuel ran off the road edge along a line that is marked by visible darkness. Some liquid spill is shown to have flowed to the opposite side as well, as indicated by the finger pattern pointing to the bottom of the photo. By the pattern, it looked like much less fuel flowed to the opposite road edge. Because relatively little fuel appeared to be lost to the opposite road edge, and the road is essentially impenetrable for the brief duration of the spill, it is supposed that most of the fuel ran off along the 30-ft road edge and into the soil near the top of the photo.

Using the picture, it was determined that the total spill area was 2,700 $ft^2$ (road plus roadside), and the area of the wetted soil above the road was 1,650 $ft^2$. Given the site is along hills close to a river and with desert like plants, it is believed the soil is sandy. From the spill modeling theory presented, it is known that an estimate of the spillage rate is needed to attempt to link the observed area with the amount spilled. Thus, an explanation for the spill rate is needed next.

Given the wetted soil area of 1650 $ft^2$ (153.3 $m^2$) and supposing a soil porosity of 0.3 and a permeability of typical sands ($1\times10^{-6}$ $cm^2$), the time required to reach a soil profile depth able to hold the spill volume (2000 gal) was estimated. When spread over 1650 $ft^2$, the full spill volume would saturate the soil to a depth of 16.5 cm. The viscosity of JP8 jet fuel is about twice that of water, or 2.05 cp, and has a density of 0.84 kg/L. Therefore, JP8 is subject to less conduction rate than water, with JP8's saturated liquid conductivity in this sand being about 0.04 cm/sec. Moving downward or infiltrating over this measured area under saturated conductivity, it would have taken the liquid volume about 123 seconds to fill the spill area. This time was used as the possible slowest release rate under the circumstances.

Note that the picture shows the tank trailer standing on its wheels, and during the spill, the tank was believed turned on its side before being righted some time later when the photo was taken. In any case, it did not seem unreasonable that 2000 gal could have gushed out a port in about 2 minutes. This corresponds to a release rate equal 16.3 gal/sec. (Note that other spill scenarios without definite information can be speculated, such as subsurface conduction horizontally of liquid through a shallow soil layer on a relatively impermeable subsurface base.)

Using these assumptions, the spill scenario was simulated with a release rate of 16.3 gal/sec. Also, a release rate of 55 gal/sec was used to bound the problem and determine the consequences. It was also presumed that the soil surface was only slightly tilted downward from the road edge, or nearly a level surface.

Figure 5.2 shows the amounts of fuel on the surface and total spilled at any time.

Notice in Figure 5.2 that the amount standing on the surface appears to reach a steady condition with infiltration into the subsurface. At no time during the spill is the surface volume more than 400 gal.

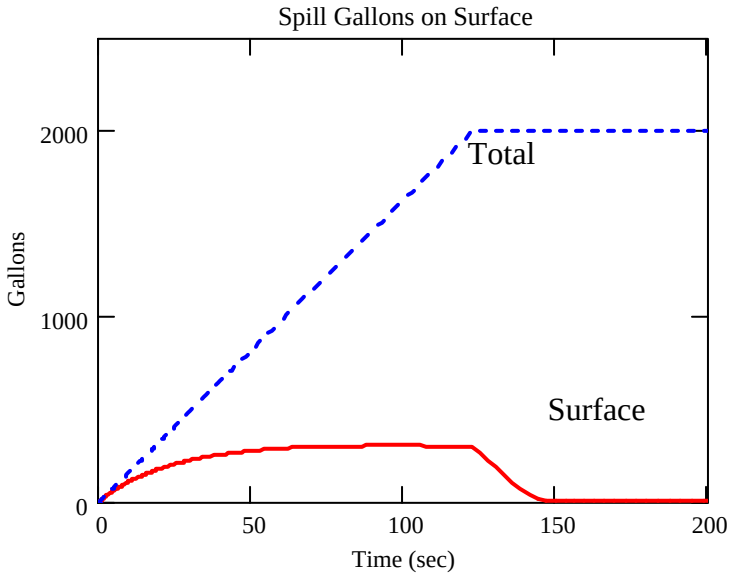


**Figure 5.2. Spill Volume on Surface of Soil and Total. Spill rate is 16.3gal/sec.**

Figure 5.3 shows how the spill is distributed with time.

During a spill, the area cover on the surface or visible spill area is dynamic and changing, whereas the volume below the surface that becomes wetted remains that way. That is, area on the surface represents liquid with a non-vanishing depth above the surface. The area involved below the surface is what remains as a visible maximum wetted area. This assumes that the fuel residual does not rapidly evaporate near the surface. In Figure 5.3, given the line of release along the road (30 ft), the width of the spreading is greater than the length. Width is measured parallel to the road edge.

In contrast, for purposes of determining sensitivity to conditions, Figure 5.4 shows the result for the faster release rate of 55 gal/sec. This yields less than 40 seconds to dump 2000 gal.

Clearly, by Figure 5.4 the faster release rate produces a much larger area than observed. So apparently the slower release or even less fast given that 3000 gal was actually lost is more consistent with the site photo.

This example shows that spill area can not be identified uniquely with the volume involved unless the spill rate is known as an essential piece of information. Of course, the permeable nature or properties of the substrate must be known also, presuming the liquid can be easily identified, say by its spectroscopy. But given that the spill volume is known approximately, along with substrate and liquid properties, how long the spill lasted can be estimated. Clearly, during an accident of this size, there was not much time to stem the loss.

For this simulation, no credit was given to capillary suction for imbibing the liquid more rapidly as it spread. With capillary suction at the wetting front included and a greater amount spilled (3000 gal), it is possible that a similar spill area could be predicted. This conclusion, however, still depends on the unknown release-rate situation.

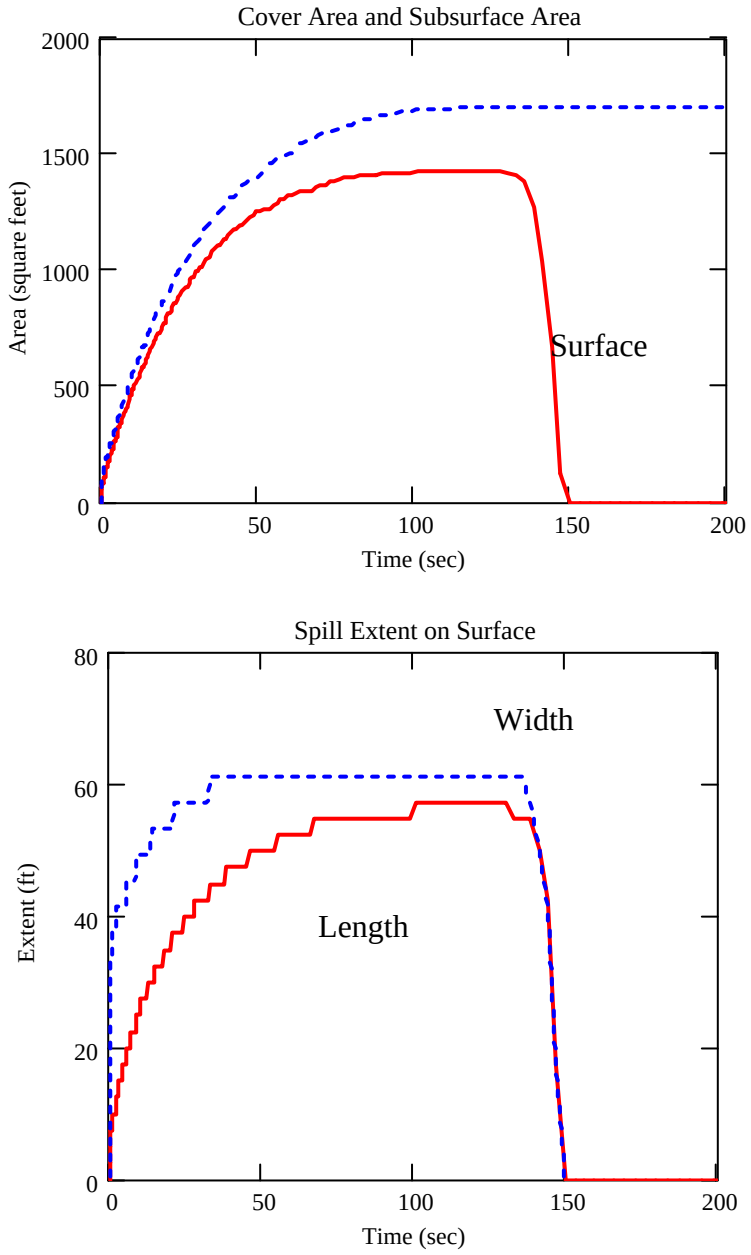


**Figure 5.3. Spill Area Covered over Time. Spill rate is 16.3gal/sec. Cover area below the surface of first graph is shown with blue dash line.**

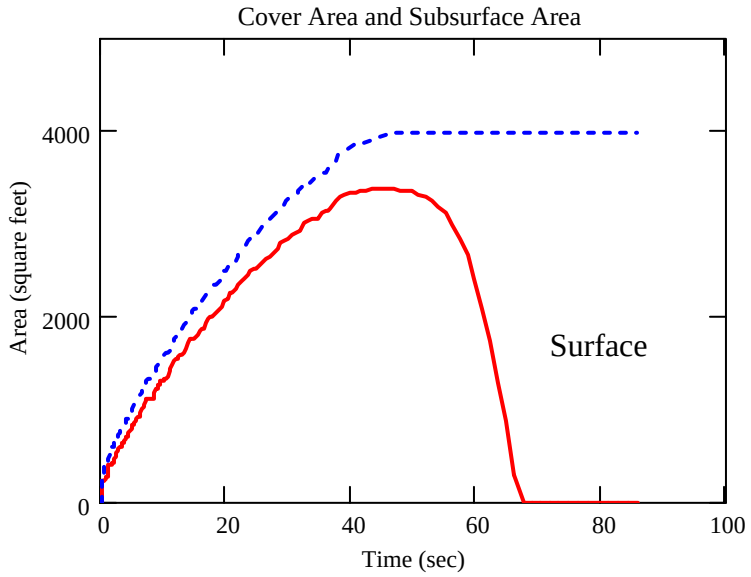


**Figure 5.4. Spill Area on Surface for 55 gal/sec**

More importantly, no credit was given to the surface roughness of the spill area. The model is for spills on ideal flat permeable surfaces. When the liquid has reached a point where its depth is only a fraction of a centimeter while the surface has imperfections greater than a centimeter height, the flow would be impeded and then controlled by the directions of groves and depressions. The overall downhill slope is also very major in controlling the spill-area shape. It is known that a slight tilt of only a degree or more will create extensive elongation of the spill plume. Given the appearance of the spill photo, a nearly flat surface was presumed so that elongation away from the road edge was not predicted. Note also that if the point of presumed spill onto the road pavement were known and the slope from the road crest known, then given the length of the wetted road edge, it could have been possible to make another estimate of how rapidly the release happened. This estimate would take advantage of the known steady spill distribution produced on an impermeable surface as the liquid exits along an edge of known length. However, the objective of this demonstration was to speculate on the spreading over a soil surface for a substantial size spill that could not be easily done in a laboratory.

# 6.0 Conclusions

This report concludes that spills on flat, level, or tilted permeable soil surfaces can be conceptually modeled using gravity current theory coupled with a simple liquid infiltration model based on the Green-Ampt formulation. The important parameter of the suction head at the wetting front can be estimated to better represent capillary imbibition of liquid during surface spreading. However, the Green-Ampt model uses the presumption that this front suction head is constant in time during infiltration, whereas the front suction head was found to decrease with time. Ultimately, a more accurate or true infiltration model should replace the Green-Ampt model in the spreading model. Nevertheless, the spreading model demonstrates the detailed coupling of dynamics between over-the-surface spreading and infiltration into a soil substrate.

If a spill involves a sufficient volume, a steady state balance of flow across a surface and into the sub-soil can occur, depending on the release rate and permeability of the soil surface. However, the model can equally well describe other complicated dynamic coupling between the overland and subsurface flows.

A real life example, a roadway spill, showed that the spill volume must be related to spill area covered through the release rate as a critical boundary condition. However, the model can be used to speculate about relationships of unknown spill variables.

This model is not experimentally validated at this juncture, being mainly a theoretical mathematical tool. Experiments need to be performed under controlled and specified conditions to determine how accurate or true the model's formulation is when applied. There are many real-world circumstances that can invalidate the model's simplified presumptions. Roughness or topography of the soil surface and its influence is one supposed key circumstance. The importance of roughness, of course, depends on the scale of the spill. If the depth of roughness is large compared to the volume spilled, then possibly an entirely different modeling concept needs to be employed to assess physical relationships.

The liquids and soils listed here with their properties are given as examples that are intended to be used in confirmation experiments to test the validity of the model and to develop its mathematical formulation further as needed. At the same time, the model simulations like those given in this report will be used to help design experimental tests of an appropriate size.

It is expected that experiments will reveal when unstable and irregular flow conditions may prevail for given liquids and soils. When the flow behavior and the geometry of spreading are not theoretically ideal, then a more advanced spill model will have to be formulated.

Presently, the spill model at least gives an estimation of the dynamical relationships between the physical parameters of the liquids and soils reported.

# 7.0 References


Acton JM, HE Huppert, and MG Worster. 2001. "Two-dimensional viscous gravity currents flowing over a deep porous medium." *Journal of Fluid Mechanics* 440:359-380.

Beilstein Database. Beilstein Institut zur Foerderung der Chemischen Wissenschaften licensed to Beilstein GmbH and MDL Information Systems GmbH.

Brilis GM, CL Gerlach, and RJ van Waasbergen. 2000. "Remote sensing tools assist in environmental forensics. Part I: Traditional methods." *Environmental Forensics* 1(2):63-67.

Chen S, PF Low, JH Cushman, and CB Roth. 1987. "Organic compound effects on swelling and flocculation of Upton montmorillonite." *Soil Science Society of America* 51:1444-1450.

Design Institute for Physical Properties Database (DIPPR). Brigham Young University, Provo, UT.

Fingas MF, and CE Brown. 1997. "Review of oil spill remote sensing." *Spill Science & Technology Bulletin* 4(4):199-208.

Gee GW, RR Kirkham, JL Downs, and MD Campbell. 1989a. *The field lysimeter test facility (FLTF) at the Hanford site: Installation and initial tests*. PNL-6810. Pacific Northwest Laboratory, Richland, WA.

Gee GW, ML Rockhold, and JL Downs. 1989b. *Status of FY 1988 soil-water balance studies on the Hanford site*. PNL-6750. Pacific Northwest Laboratory, Richland, WA.

Graber WR, and U Mingelgrin. 1994. "Clay swelling and regular solution theory." *Environmental Science and Technology* 28:2360-2365.

Green WH, and GA Ampt. 1911. "Studies on soil physics: I. Flow of air and water through soils." *Journal of Agricultural Science* 4:1-24.

Helmy AK, EA Ferreiro, and SG de Bussetti. 2003. "The surface energy of montmorillonite." *Journal of Colloid and Interface Science* 268:263-265.

Hussein M, M Jin, and JW Weaver. 2002. "Development and verification of a screening model for surface spreading of petroleum." *Journal of Contaminant Hydrology* 57:281-302.

Li D, and AW Neuman. 1990. "A reformulation of the equation-of-state for interfacial tensions." *Journal of Colloid and Interface Science* 137:304-307.

Lister JR. 1992. "Viscous flows down an inclined plane from point and line sources." *Journal of Fluid Mechanics* 22: 631-653.

Luckner L, MTh van Genuchten, and DR Nielsen. 1989. "A consistent set of parametric models for the two-phase flow of immiscible fluids in the subsurface." *Water Resources Research* 25:2187-2193.

Neuman SP. 1976. "Wetting front pressure head in the infiltration model of Green and Ampt." *Water Resources Research* 12:564-566.

Parker JC, JB Kool, and MTh van Genuchten. 1985. "Determining soil hydraulic properties from one-step outflow experiments by parameter estimation: II. Experimental studies." *Soil Science Society of America Journal* 49:1354-1359.

Schroth MH, SJ Ahearn, JS Selker, and JD Istok. 1996. "Characterization of miller-similar silica sands for laboratory hydrologic studies." *Soil Science Society of America Journal* 60:1331-1339.

Simmons CS, JM Keller, and JL Hylden. 2004. *Spills on flat inclined pavements*. PNNL-14577, Pacific Northwest National Laboratory, Richland, WA.

Simmons CS, and JM Keller. 2003. *Status of models for land surface spills of nonaqueous liquids*. PNNL-14350, Pacific Northwest National Laboratory, Richland, WA.

Theriault J-Marc, JO Jensen, A Samuels, A Ben-David, C Gittings, and W Marinelli. 2001. "Passive standoff detection of surface contaminants: Modeling the spectral radiance." In *Proceedings of the SPIE Conference on Instrumentation for Air Pollution and Global Atmospheric Monitoring*, Boston MA, October 31–November 2, 2001.

van Genuchten MTh. 1980. "A closed-form equation for predicting the hydraulic conductivity of unsaturated soils." *Soil Science Society of America Journal* 44:892-898.

White MD, M Oostrom, and RJ Lenhard. 1995. "Modeling fluid flow and transport in variably saturated porous media with the STOMP simulator. 1. Nonvolatile three-phase model description." *Advances in Water Resources* 18(6): 353-364.

# Distribution

**No. of Copies**

**OFFSITE**

7 National Geospatial-intelligence Agency
Innovision, Sensor Physics (IJ) DN MS-15
12310 Sunrise Valley Dr.
Reston VA 20191
Attn: Chris Simi (5 copies)
Ernie Reith
Jeff Mirick

3 National Geospatial-intelligence Agency
Innovision, Sensor Physics (IJ) MS N-06
1200 First St. SE.
Washington DC 20303
Attn: Bryan Albers
Herb Mitchell
Ron Holmes

**No. of Copies**

**ONSITE**

15 Pacific Northwest National Laboratory

| | |
|---|---|
| J.L. Hylden (10) | K8-41 |
| C.S. Simmons (3) | K9-33 |
| J.M. Keller (2) | K9-36 |